

Impact of Capacitive Effect and Ion Migration on the Hysteretic Behavior of Perovskite Solar Cells

Bo Chen,^{*,†} Mengjin Yang,[‡] Xiaojia Zheng,[†] Congcong Wu,[†] Wenle Li,[§] Yongke Yan,[†] Juan Bisquert,^{*,||,⊥} Germà Garcia-Belmonte,^{||} Kai Zhu,^{*,‡} and Shashank Priya[†]

[†]Center for Energy Harvesting Materials and System, Virginia Tech, Blacksburg, Virginia 24061, United States

[‡]Chemistry and Nanoscience Center, National Renewable Energy Laboratory, Golden, Colorado 80401, United States

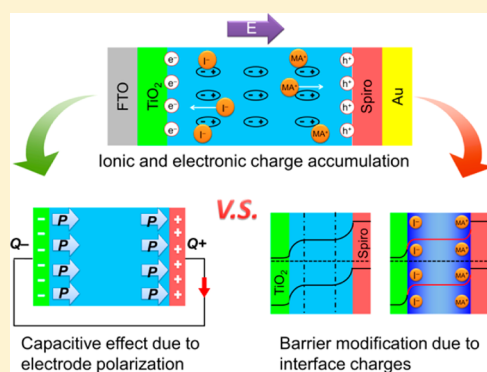
[§]Chemical Engineering, Virginia Tech, Blacksburg, Virginia 24061, United States

^{||}Institute of Advanced Materials (INAM), Universitat Jaume I, 12006 Castelló, Spain

[⊥]Department of Chemistry, Faculty of Science, King Abdulaziz University, Jeddah 21589, Saudi Arabia

S Supporting Information

ABSTRACT: In the past five years, perovskite solar cells (PSCs) based on organometal halide perovskite have exhibited extraordinary photovoltaic (PV) performance. However, the PV measurements of PSCs have been widely recognized to depend on voltage scanning condition (hysteretic current density–voltage [J – V] behavior), as well as on voltage treatment history. In this study, we find that varied PSC responses are attributable to two causes. First, capacitive effect associated with electrode polarization provides a slow transient non-steady-state photocurrent that modifies the J – V response. Second, modification of interfacial barriers induced by ion migration can modulate charge-collection efficiency so that it causes a pseudo-steady-state photocurrent, which changes according to previous voltage conditioning. Both phenomena are strongly influenced by ions accumulating at outer interfaces, but their electrical and PV effects are different. The time scale for decay of capacitive current is on the order of seconds, whereas the slow redistribution of mobile ions requires several minutes.



Organometal halide perovskite solar cells (PSCs) have become one of the most promising photovoltaic (PV) devices for solar energy harvesting.^{1–4} The power conversion efficiency (PCE) has increased from 3.8% to 20.1% in the past five years.^{5–8} Moreover, the energy payback time for perovskite solar modules has been reported as less than a half year.⁹ However, PSCs generally present a different response between forward scan and reverse scan during photocurrent density–voltage (J – V) characterization. The J – V hysteresis behavior has been observed in a variety of device architectures: PSCs on mesoporous Al_2O_3 , PSCs on mesoporous TiO_2 with perovskite capping layer, planar PSCs on compact TiO_2 , hole-transporter materials (HTM)-free PSCs, inverted polymeric PSCs, and perovskites with different organic cations and halides.^{10–17} The J – V response of PSCs is influenced by the scan direction, rate, voltage range, precondition, and device architecture.^{18–27} This anomalous J – V hysteresis behavior makes it difficult to correctly evaluate the performance of PSCs.^{28,29} In addition, the dependence of performance on previous treatments of the device raises serious concerns for the long-term stability of the solar cell operation.¹⁸

The origin of the J – V hysteresis behavior is still under debate and has been proposed to originate from the capacitive effect due to very large values of photoinduced dielectric

permittivity,^{18–21} dynamic charge trapping and detrapping process,^{25–27} or band bending due to ion migration and ferroelectric polarization.^{30–41} Specifically, Bisquert and Park et al. attributed the dynamic photovoltage decay to the photoinduced large dielectric permittivity and corresponding large capacitive effect.^{19–21} McGehee et al. reported the impact of a slow photocurrent transient process on J – V response under applied switching voltage,¹⁸ which was speculated to be caused by the ferroelectric response or photoinduced ion migration of perovskite. Snaith et al. proposed that the charge traps underwent a filling process under forward bias and a detrapping process under reverse bias, which could influence the extraction of the photoexcited carriers.^{24,26} They found that the electron transfer from perovskite to compact TiO_2 was not very effective, and coating TiO_2 with C_{60} -SAM (an electron acceptor) can significantly reduce the J – V hysteresis behavior.²⁶ Huang et al. also attributed the hysteretic effect to the charge trapping/detrapping process of the trap states on the surface and grain boundaries of the perovskite materials; the fullerene passivation of those trap states could successfully

Received: October 6, 2015

Accepted: November 9, 2015

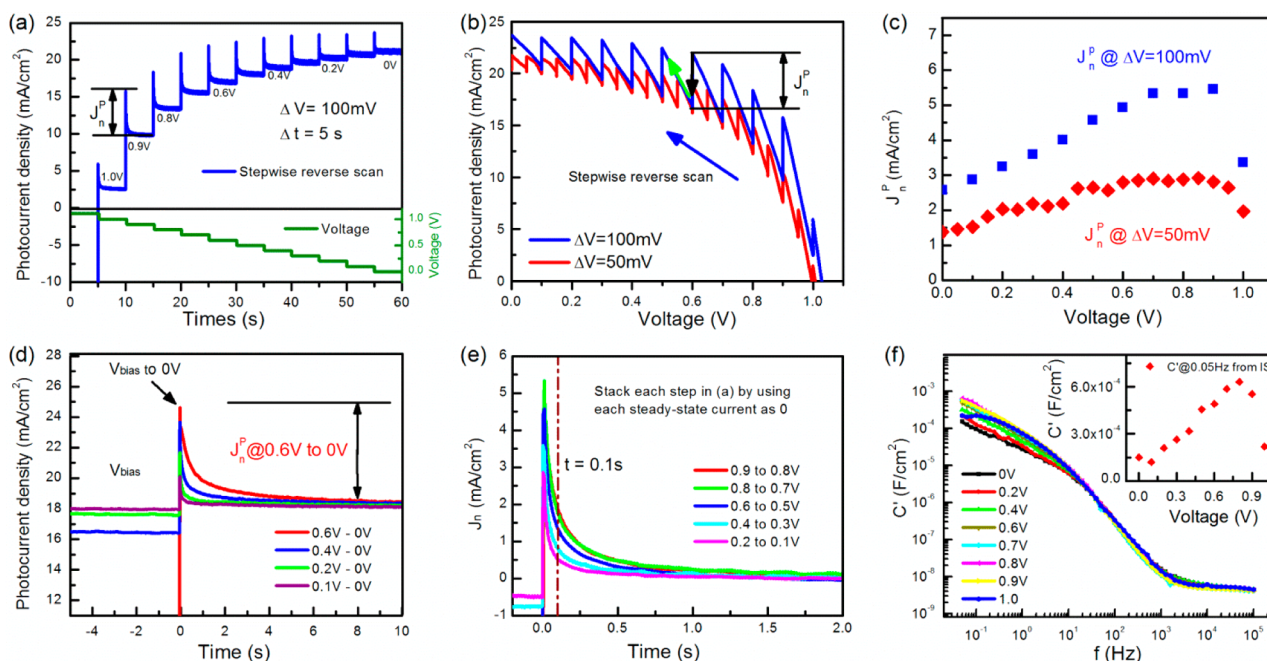


Figure 1. (a) Time-dependent photocurrent response under stepwise reverse scan with 100-mV step size and 5-s step time. (b) J - V response under stepwise reverse scan from 1.1 to 0 V with 100-mV and 50-mV step size; step time is 5 s. (c) The relation of peak nonsteady-state photocurrent J_n^p with applied bias. (d) Nonsteady-state photocurrent when switching applied bias from different V_{bias} to 0 V. (e) Decay of dynamic nonsteady-state photocurrent $J_n(t)$ with time during stepwise reverse scan in (a). (f) Capacitance (C' , real part) as a function of frequency at different bias under illumination; the inset is the relation of C' with applied bias obtained from IS measurement at 0.05 Hz.

eliminate the J - V hysteresis.²⁵ However, Snaith et al. found that the trapping process occurs at time scales on the order of 10^{-5} s, and they suggested that the charge trapping is not the cause of hysteresis occurring on time scales greater than milliseconds.⁴² The activation energies for ion migration in $\text{CH}_3\text{NH}_3\text{PbI}_3$ thin films are calculated to be around 0.45 to 0.58 eV from first-principles,^{30–32} which indicates the possibility of ion migration in PSCs. The ion migration under an external electric field is speculated to cause accumulation of mobile ions at the interfaces, which modulates the net built-in electric field and also modifies the injection barriers for electronic carriers.^{33–37} The slow redistribution process of ion migration may also be responsible for the J - V hysteresis.^{33–37} Moreover, the switching of ferroelectric polarization during J - V characterization has also been proposed to regulate the band structure and create hysteresis for the perovskite solar cells.^{38–41}

The presence of a large capacitance at low frequency in PSCs has been observed by Juarez-Perez et al.²¹ Furthermore, it has been shown that such capacitance provides hysteresis behavior in the dark that is characterized by symmetric opening of the J - V curve around the steady-state curve, where all scan-dependent curves converge at very low scan rate.²² However, capacitive currents in operating conditions at one-sun illumination have yet to be shown conclusively. In addition, there is considerable evidence that the hysteresis phenomena and bias pretreatment dependence of the J - V curves cannot be ascribed solely to capacitive response. Moreover, radical modifications of J - V response can be realized such as the inversion of the diode curve by poling.⁴³ These phenomena must be related to a strong modification of the PV mechanism very likely associated with the ion drift induced by photovoltage or polarization.

In this study, we aim to find the dominant origin—or origins, as they may be diverse—of the hysteretic J - V response. We

investigate whether the nonsteady-state photocurrent during J - V characterization is a capacitive current. The correlation between the slow dynamic transient of nonsteady-state photocurrent and capacitive current is confirmed by stepwise scanning, the dynamic J_{SC} transient process, and impedance spectroscopy (IS). Next, we propose an approach to quantitatively estimate the value of ion-migration-induced band-shift. The analysis indicates a huge band-shift, which challenges the hypothesis of an ion-migration mechanism. The dynamic J_{SC} transient process after electric poling differentiates the transient time scales between the ion migration and capacitive current, revealing that it is the capacitive effect that dominates the emergence of J - V hysteresis. Further, the difference of J_{SC} under forward and reverse scans is used to elucidate the dominant mechanism contributing to J - V hysteresis.

Capacitive Effect during Voltage Variation. We fabricated a planar perovskite solar cell on compact TiO_2 (cp- TiO_2) with 500 nm $\text{CH}_3\text{NH}_3\text{PbI}_3$ film as the light-absorber layer and 150 nm Spiro-OMeTAD as the HTM layer, as described in the scanning electron microscopy (SEM) image shown in Figure S1. Photocurrent for PSCs can be divided into two parts: steady-state photocurrent J_0 and nonsteady-state photocurrent $J_n(t)$. The steady-state J_0 is due to the diode characteristic response of the extraction and recombination of photo-generated charges. The nonsteady-state photocurrent $J_n(t)$ changes with time, and the first task of this paper is to identify its origin.

The J - t curve in Figure 1a presents the evolution of nonsteady-state photocurrent in response to stepwise variation of the applied voltage from 1.1 to 0 V with $\Delta V = 100$ mV. A peak nonsteady-state photocurrent emerges whenever applied bias is reduced. Considering that all photocurrent reaches the steady-state J_0 at the end of each step, the variation of

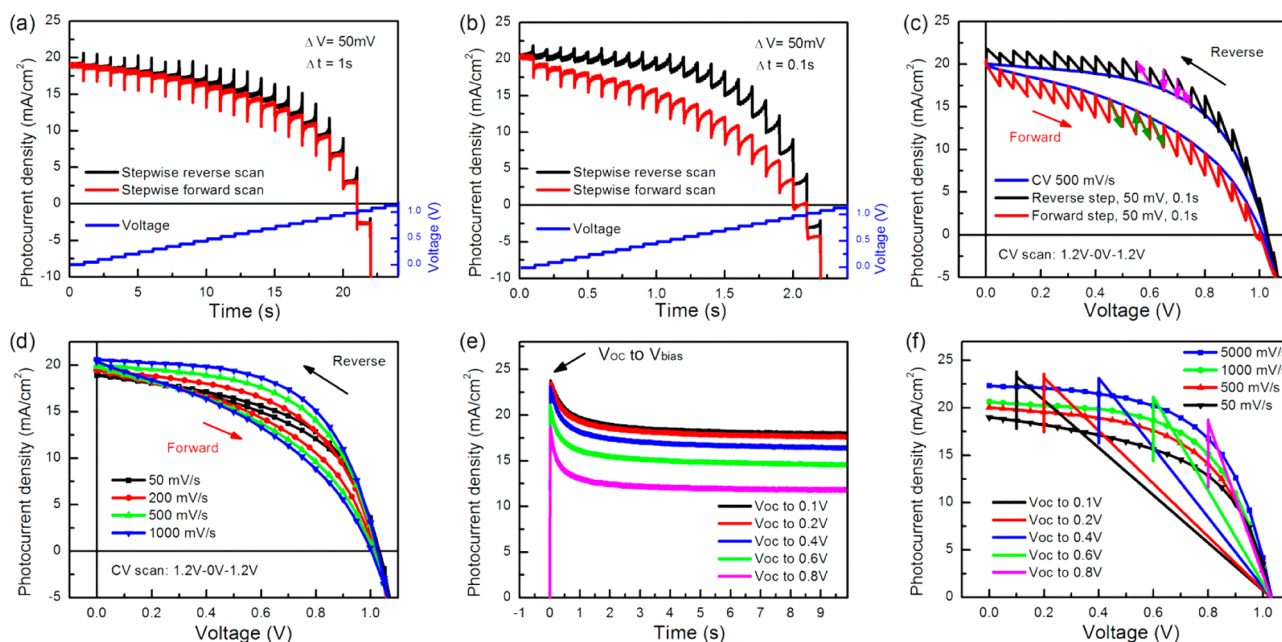


Figure 2. Time-dependent photocurrent response under reverse and forward stepwise scans with (a) 1 s step time and (b) 0.1 s step time. (c) J - V response for the CV scan with 500 mV/s and corresponding stepwise scan. (d) J - V response for PSCs with different CV scan rates. (e) Dynamic photocurrent transient when switching the applied voltage from open-circuit voltage (V_{oc}) to different bias. (f) J - V response for the different reverse scans and dynamic photocurrent transient in (e).

photocurrent $\Delta J(t)$ is equal to the peak value of nonsteady-state photocurrent J_n^p , which is shown more clearly in the J - V plot in Figure 1b. If step size ΔV is reduced from 100 mV to 50 mV, J_n^p at each applied bias decreases to about half of the corresponding value under $\Delta V = 100$ mV (e.g., J_n^p reduces from 4.01 to 2.19 mA/cm² at 0.4 V), as shown in Figure 1c. Moreover, it is interesting to note that the peak capacitive current J_n^p not only depends on ΔV but also changes with the applied bias. The detailed J_n^p - V_{bias} relation is shown in Figure 1c for both a 100 mV and 50 mV stepwise scan. J_n^p increases with the increase of V_{bias} and reaches the maximum value at 0.7–0.9 V applied bias. To further explore the relationship between non-steady-state photocurrent and ΔV , the perovskite solar cell was first stabilized at different V_{bias} values for 5 min and then switched to a short-circuit condition (Figure 1d). In this case, the peak J_n^p enlarges with the increase of ΔV . In Figure 1e, we stack all J - t curves of each step during the stepwise scan by using the steady-state current at the end of each step as a reference. This provides the decay of nonsteady-state current $J_n(t)$ with time. The decay half-time for the slow transient process of $J_n(t)$ is around 0.1 s.

Considering the dependence of the nonsteady-state photocurrent $J_n(t)$ on voltage change and its slow transient decay properties, the nonsteady-state photocurrent might be attributed to the capacitive current $J_{cap}(t)$. The capacitive effect corresponds to the low-frequency capacitance, where the frequency must be associated with the reciprocal time scale of voltage step. At very low frequency, the PSC shows very large capacitance (Figure 1f). The capacitance at 0.05 Hz in the IS measurement is displayed in the inset of Figure 1f. In addition, the capacitance changes under external bias as confirmed in Figure 1f. Low-frequency capacitance enlarges with the increase of V_{bias} and displays maximum values at an applied bias of ~ 0.8 V, which is consistent with the J_n^p - V_{bias} relation in Figure 1c. Moreover, the relatively high capacitive

current at ~ 0.8 V applied bias may be the reason that J - V curves typically display pronounced hysteresis at ~ 0.8 V.

Due to the slow transient process of the capacitive current, the nonsteady-state capacitive current can influence the J - V response until it is completely decayed (Figure 2). When the step interval time is 1 s, which is ~ 10 times of the decay half-time, the photocurrent is able to reach the steady-state J_0 , then the J - V response demonstrates negligible hysteresis as shown in Figure 2a, and the device demonstrates short-circuit current density (J_{sc}) of 18.95 mA/cm², V_{oc} of 1.03 V, fill factor (FF) of 53.3%, and PCE of 10.4% (Figure 2d, 50 mV/s scan). However, when the step interval time is reduced to 0.1 s, a significant fraction of capacitive current still exists at the end of each step, as shown in Figure 1e. In this case, the negative remanent capacitive current results in the photocurrent under forward scan being lower than the steady-state photocurrent, whereas the photocurrent under reverse scan is higher than the steady-state photocurrent due to positive remanent capacitive current (as demonstrated in Figure S2). As a result, a remarkable difference emerges between the forward and reverse scans at fast scan rate, as shown in Figure 2b. In addition, the J - V curve is symmetrically opened around the steady-state curve, as shown in Figure 2d, which is the mark of a capacitive current (which changes sign when the direction of scan rate is inverted). Such capacitive current, however, will not grow indefinitely when the scan rate is increased. The reason is that the capacitance decreases at increasing frequency, by several orders of magnitude, as shown in Figure 1f. Therefore, at extremely large frequencies, capacitive hysteresis will be suppressed, as observed previously.³⁴ The transient capacitive current depends on the capacitance and voltage variation:

$$J_{cap} = \frac{\Delta Q}{A \Delta t} = \frac{C \times \Delta V}{A \Delta t} \quad (1)$$

Considering $\Delta V = 50$ mV, $\Delta t = 0.1$ s, cell active area $A = 0.1$ cm², and C around 1.5×10^{-4} to 6.3×10^{-4} F/cm², we estimate

the peak value of capacitive current is 0.75–3.15 mA/cm², which is consistent with the order of peak capacitive current value in Figure 2.

In the case of a fast scan rate, the nonsteady-state photocurrent cannot decay sufficiently, and each photocurrent density data point would be close to the peak value of nonsteady-state photocurrent density. These values can be measured by directly switching applied voltage from V_{oc} to corresponding V_{bias} . Therefore, we recorded the dynamic photocurrent by switching bias from V_{oc} to V_{bias} in Figure 2e. Figure 2f demonstrates the corresponding J – V curve, denoted as J – $V@V_{oc}-V_{bias}$. All J – V curves for linear reverse scans are located between the maximum and minimum values of J – $V@V_{oc}-V_{bias}$. Therefore, the maximum point of each J – $V@V_{oc}-V_{bias}$ suggests the highest possible artificial PCE under fast reverse scan. The minimum point of each J – $V@V_{oc}-V_{bias}$ indicates the steady-state J – V response at each applied bias.

It has been demonstrated in a recent paper that leakage and capacitive currents can be decoupled in a varying scan rate experiment.²² The leakage current dominates the dark J – V curve at low voltages only in the case of very slow scan rates (steady-state conditions), while the capacitive current masks the leakage as the scan rate is increased. To differentiate the leakage current from the capacitive current, we carried out the J – V measurement under dark conditions both with linear scan and stepwise scan. There is no photocurrent under the dark condition, so the dark J – V measurements can be used to evaluate the impact of leakage current (if there is any) on the hysteresis behavior. As we can see in Figure S4, the dark current under stepwise scan also demonstrates a peak nonsteady-state current, but the value of dark current is less than 0.02 mA/cm² when the applied voltage is less than 0.8 V. This demonstrates that there is no obvious influence of the leakage current on the hysteresis behaviors.

Non-Steady-State Photocurrent Due to Ion Migration. In addition to the capacitive effect, ion migration has also been speculated to create nonsteady-state photocurrent due to the slow redistribution process of mobile ions under an external electric field.^{32,34–37} The accumulation of mobile ions at the interface under an external electric field is proposed to change the electron/hole injection barrier and create the band bending, which influences the extraction efficiency of photoexcited electrons and holes.^{32,34–37} If the band bending has an equivalent effect as the change of net built-in electric field due to bias shift, then we propose a method to quantitatively estimate the ion-migration-induced bias-shift by considering the dominant impact of ion migration on the formation of nonsteady-state photocurrent.

As shown in Figure S5, we introduce V_{mn} to represent ion-migration-induced equivalent bias-shift (or band-bending) under different applied bias of V_n ($n = 0, 1, 2, \dots$); the equivalent bias-shift V_{mn} is determined by the potential difference ($\Delta V = V_{oc} - V_n$). The equilibrium effectively applied bias (V_{bias}') for PSCs after ion migration is $V_{bias}' = V_n + V_{mn}$. At forward stepwise scan, when the applied bias increases from V_0 to V_1 , the V_{bias}' first jumps immediately from $V_0 + V_{m0}$ to $V_1 + V_{m0}$ (due to the immediate increase of applied bias and slow response of ion migration), and then gradually reduces from $V_1 + V_{m0}$ to $V_1 + V_{m1}$ resulting from the slow variation of V_{mn} associated with ion migration. This is accompanied by a nonsteady-state photocurrent increasing gradually from $J@V_1 + V_{m0}$ to $J@V_1 + V_{m1}$, as shown in Figure S5a. If the nonsteady-state photocurrent is dominated by the ion-

migration-induced band bending, we propose to introduce the stepwise scan to quantitatively estimate the equivalent bias-shift V_{mn} at different applied bias in Figure S5c. Consider the obvious change of steady-state photocurrent at each step from 0 V to V_{oc} ; the same value of photocurrent should indicate the same value of corresponding V_{bias}' . Using this approach, we can get a rough relation of V_{mn} with applied bias, as shown in Figure S5d. The accumulation of mobile ions at an interface can lead to a reduction of net potential difference by $\sim 70\%$, which leaves a net built-in potential difference ($\Delta V' = V_{oc} - V_{bias}'$) of less than 0.3 V under the applied bias between 0 V and V_{oc} . This huge potential shift is difficult to generate within the PSC devices, as it would significantly deteriorate the PV performance. This challenges the possibility of ion migration to change the band bending in bulk to create J – V hysteresis behavior. However, the modification of injection barriers at the perovskite/electrode interface due to ion migration might still be a plausible explanation.

Capacitive Effect versus Ion Migration. To differentiate the impact of capacitive effect and ion-migration-induced effects on J – V hysteresis more clearly, we carried out the dynamic J_{sc} transient process analysis after electric poling to understand their respective characteristic time scales affecting J – V measurement. If the J – V hysteresis behavior originates from the ion migration, then the electric poling should be able to create a large concentration of accumulated mobile ions at the interface that increases the band-bending or barrier-modification effect. We electrically poled the perovskite solar cell for 30 s under dark condition with -1 V or -2 V, and then short-circuited the sample for 1 min to eliminate the electric-charge accumulation before J – V characterization. The dynamic J_{sc} photoresponse after electric poling is then recorded by switching the applied voltage from V_{oc} to short-circuit condition.

As shown in Figure 3a, the J_{sc} transient processes after poling demonstrate two dynamic processes with different time scales: (i) pulse nonsteady-state photocurrent exhibits fast decay time (~ 1 s) and the photocurrent maintains the steady-state J_{sc} in the next 10 s, and (ii) J_{sc} for poled sample is in pseudo-steady-state and gradually increases to the same value as the unpoled sample in 3 min. The slow recovery of J_{sc} for the poled samples in several minutes cannot be explained by capacitive effect, but can be ascribed to the slow redistribution process of the ion migration. Moreover, if the band bending is activated by ferroelectric polarization, then it cannot recover unless the applied bias is larger than V_{oc} .^{39–41} Therefore, the possibility of ferroelectric polarization for the band-bending effect can be excluded based on the results in Figure 3a. Considering both V_{oc} and 0 V are larger than the poling bias, the equivalent bias-shift V_{mn} after poling should therefore keep decreasing under either V_{oc} or short-circuit condition, or the barrier height after poling should try to recover under either V_{oc} or short-circuit condition. Therefore, if the ion migration dominates the formation of nonsteady-state photocurrent, the photocurrent should keep increasing under either V_{oc} or short-circuit condition, and there would be no sharp decrease of photocurrent at the beginning of J_{sc} transient processes. Moreover, the ion migrations cannot explain two different time scales for the slow transient of pseudosteady-state photocurrent and the fast decay of the pulse photocurrent. We ascribe this pulse photocurrent and corresponding fast decay process to the capacitive effect due to the dynamic charging process when switching the bias from V_{oc} to 0 V.

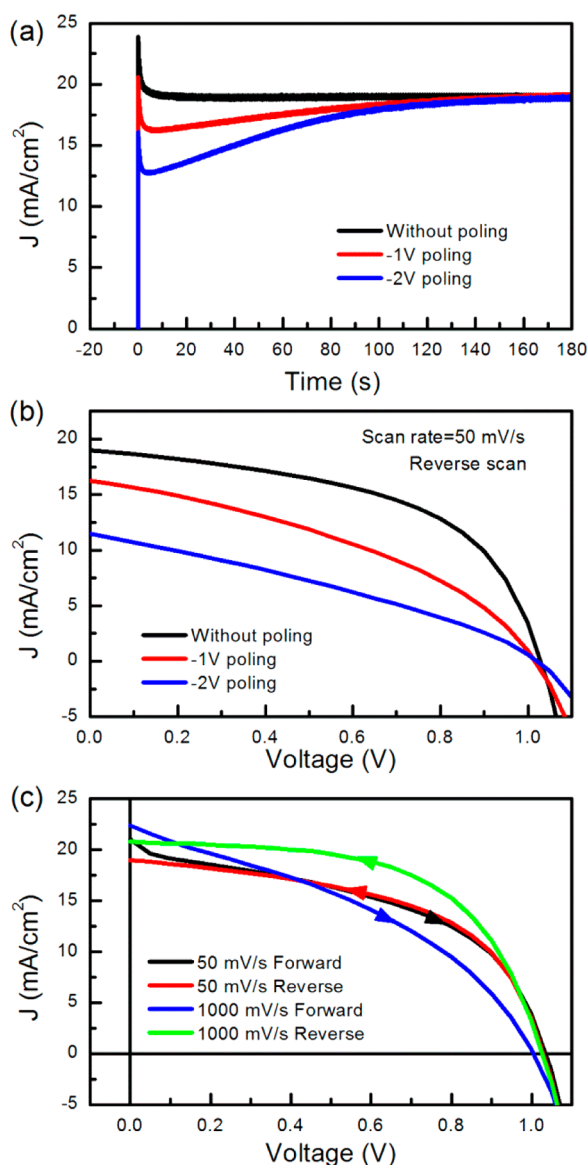


Figure 3. (a) Dynamic J_{sc} transient processes when switching bias from V_{oc} to 0 V for unpoled and poled samples. (b) J - V responses at 50 mV/s reverse scan for unpoled and poled samples. (c) J - V responses under forward and reverse scan with different scan rates.

As shown in Figure 3b, after negative poling, the photocurrent values at different applied bias during J - V scanning are significantly decreased compared to the unpoled sample. These effects cannot be explained by capacitive currents such as those shown in Figure 1. The modification of the photocurrent may be explained either by a change of the charge-collection efficiency, due to modification of band bending in the bulk perovskite layer, or by a variation of the charge-injection efficiency of the contacts. Both phenomena can be a result of the ion-migration effect. However, pretreatment and hysteresis effects have been observed to depend markedly on the type of contact, and are largely suppressed by addition of carbonaceous materials.^{26,44} Therefore, the electrical field in the bulk is not sufficient to explain variations of pseudosteady-state photocurrent, as already concluded earlier. Here, we attribute such variation to the modification of electronic injection barriers. Similarly, the impact of light soaking with different applied bias prior to J - V characterization can also lead to different

electronic injection barriers due to ion migrations, which generate different PV performance.

Another method to directly compare the capacitive effect and ion migrations is to compare J_{sc} under forward scan and reverse scan. Between short-circuit condition and V_{oc} , the forward scan first activates the negative poling, whereas the reverse scan performs the opposite. Therefore, if ion migration dominates the J - V hysteresis, the J_{sc} under forward scan should be smaller than J_{sc} under reverse scan, because the negative poling under forward scan can increase the barrier height to suppress the extraction of photoexcited charges. We performed the forward scan and reverse scan separately with the same precondition (light soaking at open-circuit condition for 1 min) at various scan rates, as shown in Figure 3c and Figure S6. Although the forward scan displays a lower PCE than that of the reverse scan, J_{sc} under forward scan is always higher than J_{sc} under reverse scan, regardless of the scan rates. This phenomenon conflicts with the prediction that the ion-migration effect dominates the J - V hysteresis, but it can be explained by the large positive capacitive current when the external circuit changes from open circuit to short circuit. Therefore, the formation of J - V hysteresis is dominated by the capacitive effect.

The large capacitive effect can be ascribed to electrode polarization due to ionic accumulation and electronic accumulation. The layer-thickness independent property of the low-frequency capacitance value indicates the interfacial mechanism of capacitance.²² The reported capacitance (and dark current) values are well explained by ions accumulating at the perovskite/contact layer interface due to ion migration, extending over a region of order 10 nm.²² Additional electronic effect induced by light exposure cannot be ignored in the final capacitive values. The capacitance increases several orders of magnitude under illumination, which shows that photoexcited electronic carriers enhance the effect. The large capacitance under illumination can be ascribed to the large interfacial electronic dipole polarization induced by accumulated electron and hole at the perovskite/electrode interface due to the inefficient extraction of photoexcited charges. Different architectures of perovskite solar cells (such as planar PSCs on cp-TiO₂, PSCs based on mesoporous TiO₂, and inverted polymeric PSCs) demonstrate different magnitudes of hysteresis. This can be ascribed to different levels of electronic dipole polarization and interfacial ionic accumulations. Because of effective electron extraction using mesoporous TiO₂, the PSCs based on mesoporous TiO₂ can avoid electron accumulation at the perovskite/TiO₂ interface. Moreover, modification of the cp-TiO₂ surface by C₆₀-SAM,²⁶ covering the CH₃NH₃PbI₃ grain boundaries by PCBM,²⁷ or using inverted PSCs with PCBM as the electron-transporter layer^{25,45} can significantly improve the electron-extraction efficiency and can also passivate the interface ionic charges. This suppresses the interfacial electronic dipole polarization and interfacial ionic accumulation, thus reducing the capacitive effect and suppressing/eliminating the corresponding J - V hysteresis behavior. The passivation effect by PCBM and C₆₀-SAM can reduce the transient time scale of capacitive current; thus, the photocurrent can quickly reach the steady-state photocurrent at each applied bias to eliminate the hysteresis phenomena. The interplay between the amount of ions and their transport properties (which depend on the crystalline quality of the perovskite film), and the interface properties concerning the ability of ion accommodation gives rise to the variety of experimental hysteretic observations.

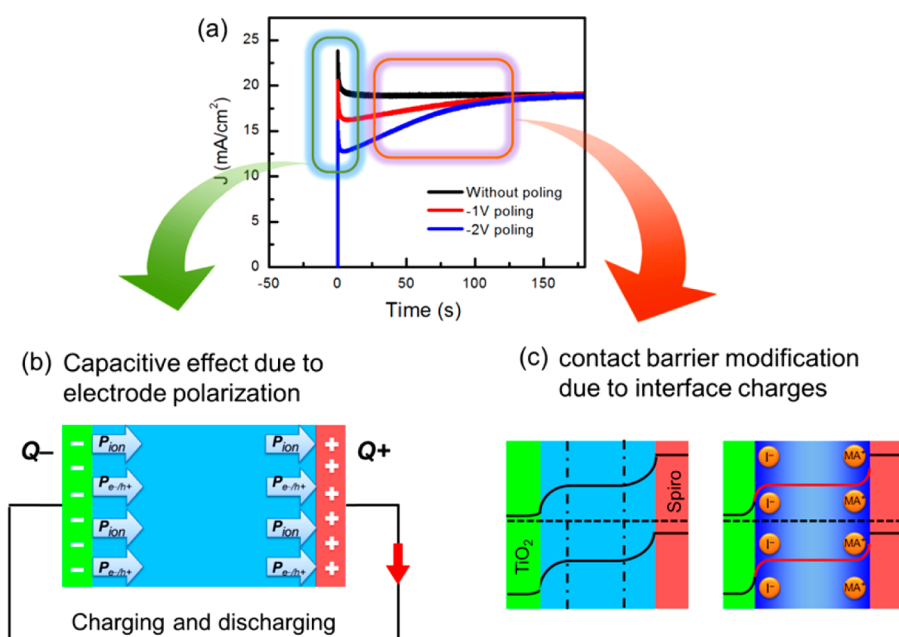


Figure 4. Schematic illustration for the origin of J - V hysteresis behavior: (a) dynamic J_{sc} transient processes with two decay time scales, (b) the influence of modifying electrode polarization on capacitive effect, and (c) the impact of contact barrier modification due to interface ionic charges.

In addition to the change of electrode polarization as shown in Figure 4b, ion migration can also cause barrier modification due to the accumulated charges at the interface, as shown in Figure 4c. In contrast to the nonsteady-state capacitive effect, the modification of interfacial barriers due to ion migration can modulate the steady-state current for the PSCs and influence the J - V response. The time scale for the ion-migration-induced barrier modification to reach equilibrium state is on the order of several minutes, whereas the time scale for the decay of the capacitive current is on the order of seconds.

Therefore, capacitive effect and ion-migration-induced injection barrier modification both have a remarkable influence on J - V response. The capacitive effect can generate a nonsteady-state photocurrent during voltage sweep, whereas the ion-migration-induced contact modification can modulate the pseudo-steady-state photocurrent. From the stepwise J - V scan in Figures 1 and 2, we know that it is the transient of nonsteady-state photocurrent with time scale on the order of seconds that causes the hysteretic J - V behavior. Thus, the capacitive effect should dominate the formation of non-steady-state photocurrent and the J - V hysteresis behavior. The ion migration would not be able to respond quickly enough to induce non-steady-state photocurrent. However, under slow scan rates, the voltage cycling itself may induce ion reorganization so that the hysteresis of the J - V curve is not symmetric around the steady-state curve, and the steady-state photocurrent is also modified. In general, a variety of combined effects may appear depending on cell properties and measurement protocol.

In summary, we have extensively analyzed the influence of both capacitive effect and ion migration on the J - V response of perovskite solar cells to understand the origin of hysteresis. The formation of nonsteady-state photocurrent and J - V hysteresis is dominated by the capacitive effect. Due to the slow decay process of capacitive current, a fast scan rate leads to smaller (or larger) photocurrent than the steady-state photocurrent due to a negative (or positive) remanent capacitive current under forward (or reverse) scan, which contributes to the J - V

hysteresis. The dynamic J_{sc} transient processes after electric poling reveal that ion migration can regulate the steady-state photocurrent due to modification of electron/hole injection barrier, whereas the redistribution of ion migration occurs at the time scale of several minutes. The capacitive effect is related to the changing of low-frequency capacitance, mainly related to electrode polarization. The dynamic J_{sc} transient process and stepwise scan provide key factors for hysteresis—decay time scale of capacitive current, value of capacitive current, and change of pseudosteady-state photocurrent density—that cannot be explained by capacitive current. With those parameters, the impact of capacitive effect and ion migration on the J - V hysteresis can be evaluated, and the accurate PV performance of the PSCs can be determined.

■ ASSOCIATED CONTENT

📄 Supporting Information

The Supporting Information is available free of charge on the ACS Publications website at DOI: 10.1021/acs.jpcllett.5b02229.

The experimental procedure of device fabrication and characterization, the SEM image for the structure of perovskite solar cells, detailed slow transient process based on either capacitive effect or ion migration, and J - V response under forward and reverse scans at different scan rate (PDF)

■ AUTHOR INFORMATION

Corresponding Authors

*E-mail: bochen09@vt.edu (B.C.).

*E-mail: bisquert@uji.es (J.B.).

*E-mail: kai.zhu@nrel.gov (K.Z.).

Notes

The authors declare no competing financial interest.

■ ACKNOWLEDGMENTS

The authors gratefully acknowledge the financial support through the U.S. Army under Contract No. W15P7T-13-C-

A910. The work at the National Renewable Energy Laboratory was supported by the U.S. Department of Energy SunShot Initiative under the Next Generation Photovoltaics 3 program (DE-FOA-0000990) under Contract No. DE-AC36-08-GO28308. S.P. and C.W. also appreciate support from the NSF I/UCRC: Center for Energy Harvesting Materials and Systems through Fundamental Research Program. The work at INAM-UJI was supported by Generalitat Valenciana project PROMETEO/2014/020.

REFERENCES

- (1) Burschka, J.; Pellet, N.; Moon, S. J.; Humphry-Baker, R.; Gao, P.; Nazeeruddin, M. K.; Grätzel, M. Sequential Deposition as a Route to High-performance Perovskite-sensitized Solar Cells. *Nature* **2013**, *499*, 316–319.
- (2) Liu, M. Z.; Johnston, M. B.; Snaith, H. J. Efficient Planar Heterojunction Perovskite Solar Cells by Vapour Deposition. *Nature* **2013**, *501*, 395–398.
- (3) Green, M. A.; Ho-Baillie, A.; Snaith, H. J. The Emergence of Perovskite Solar Cells. *Nat. Photonics* **2014**, *8*, 506–514.
- (4) Mei, A.; Li, X.; Liu, L.; Ku, Z.; Liu, T.; Rong, Y.; Xu, M.; Hu, M.; Chen, J.; Yang, Y.; Grätzel, M.; Han, H. W. A Hole-conductor-free, Fully Printable Mesoscopic Perovskite Solar Cell with High Stability. *Science* **2014**, *345*, 295–298.
- (5) Kojima, A.; Teshima, K.; Shirai, Y.; Miyasaka, T. Organometal Halide Perovskites as Visible-Light Sensitizers for Photovoltaic Cells. *J. Am. Chem. Soc.* **2009**, *131*, 6050–6051.
- (6) Kim, H. S.; Lee, C. R.; Im, J. H.; Lee, K. B.; Moehl, T.; Marchioro, A.; Moon, S. J.; Humphry-Baker, R.; Yum, J. H.; Moser, J. E.; Grätzel, M.; Park, N. G. Lead Iodide Perovskite Sensitized All-Solid-State Submicron Thin Film Mesoscopic Solar Cell with Efficiency Exceeding 9%. *Sci. Rep.* **2012**, *2*, 591.
- (7) Zhou, H. P.; Chen, Q.; Li, G.; Luo, S.; Song, T. B.; Duan, H. S.; Hong, Z. R.; You, J. B.; Liu, Y. S.; Yang, Y. Interface Engineering of Highly Efficient Perovskite Solar Cells. *Science* **2014**, *345*, 542–546.
- (8) Yang, W. S.; Noh, J. H.; Jeon, N. J.; Kim, Y. C.; Ryu, S.; Seo, J.; Seok, S. I. High-performance Photovoltaic Perovskite Layers Fabricated through Intramolecular Exchange. *Science* **2015**, *348*, 1234–1237.
- (9) Gong, J.; Darling, S. B.; You, F. Q. Perovskite Photovoltaics: Life-cycle Assessment of Energy and Environmental Impacts. *Energy Environ. Sci.* **2015**, *8*, 1953–1968.
- (10) Jeon, N. J.; Noh, J. H.; Kim, Y. C.; Yang, W. S.; Ryu, S.; Seok, S. I. Solvent Engineering for High-Performance Inorganic-Organic Hybrid Perovskite Solar Cells. *Nat. Mater.* **2014**, *13*, 897–903.
- (11) Ke, W.; Fang, G.; Wan, J.; Tao, H.; Liu, Q.; Xiong, L.; Qin, P.; Wang, J.; Lei, H.; Yang, G.; Qin, M.; Zhao, X.; Yan, Y. Efficient Hole-blocking Layer-free Planar Halide Perovskite Thin-film Solar Cells. *Nat. Commun.* **2015**, *6*, 6700.
- (12) Zhang, W.; Saliba, M.; Moore, D. T.; Pathak, S. K.; Hörantner, M. T.; Stergiopoulos, T.; Stranks, S. D.; Eperon, G. E.; Alexander-Webber, J. A.; Abate, A.; Sadhanala, A.; Yao, S.; Chen, Y.; Friend, R. H.; Estroff, L. A.; Wiesner, U.; Snaith, H. J. Ultrasoft Organic-inorganic Perovskite Thin-film Formation and Crystallization for Efficient Planar Heterojunction Solar Cells. *Nat. Commun.* **2015**, *6*, 6142.
- (13) Dharani, S.; Dewi, H. A.; Prabhakar, R. R.; Baikie, T.; Shi, C.; Yonghua, D.; Mathews, N.; Boix, P. P.; Mhaisalkar, S. G. Incorporation of Cl into Sequentially Deposited Lead Halide Perovskite Films for Highly Efficient Mesoporous Solar Cells. *Nanoscale* **2014**, *6*, 13854–13860.
- (14) Xiao, M.; Huang, F.; Huang, W.; Dkhissi, Y.; Zhu, Y.; Etheridge, J.; Gray-Weale, A.; Bach, U.; Cheng, Y.-B.; Spiccia, L. A Fast Deposition-Crystallization Procedure for Highly Efficient Lead Iodide Perovskite Thin-Film Solar Cells. *Angew. Chem., Int. Ed.* **2014**, *53*, 9898–9903.
- (15) Ono, L. K.; Raga, S. R.; Wang, S.; Kato, Y.; Qi, Y. Temperature-Dependent Hysteresis Effects in Perovskite-Based Solar Cells. *J. Mater. Chem. A* **2015**, *3*, 9074–9080.
- (16) Ryu, S.; Seo, J.; Shin, S. S.; Kim, Y. C.; Jeon, N. J.; Noh, J. H.; Seok, S. I. Fabrication of Metal-oxide-free $\text{CH}_3\text{NH}_3\text{PbI}_3$ Perovskite Solar Cells Processed at Low Temperature. *J. Mater. Chem. A* **2015**, *3*, 3271–3275.
- (17) Im, J.-H.; Jang, I.-H.; Pellet, N.; Grätzel, M.; Park, N.-G. Growth of $\text{CH}_3\text{NH}_3\text{PbI}_3$ Cuboids with Controlled Size for High-Efficiency Perovskite Solar Cells. *Nat. Nanotechnol.* **2014**, *9*, 927–932.
- (18) Unger, E. L.; Hoke, E. T.; Bailie, C. D.; Nguyen, W. H.; Bowring, A. R.; Heumüller, T.; Christoforo, M. G.; McGehee, M. D. Hysteresis and Transient Behavior in Current-voltage Measurements of Hybrid-perovskite Absorber Solar Cells. *Energy Environ. Sci.* **2014**, *7*, 3690–3698.
- (19) Kim, H.-S.; Park, N.-G. Parameters Affecting I-V Hysteresis of $\text{CH}_3\text{NH}_3\text{PbI}_3$ Perovskite Solar Cells: Effects of Perovskite Crystal Size and Mesoporous TiO_2 Layer. *J. Phys. Chem. Lett.* **2014**, *5*, 2927–2934.
- (20) Sanchez, R. S.; Gonzalez-Pedro, V.; Lee, J.-W.; Park, N.-G.; Kang, Y. S.; Mora-Sero, I.; Bisquert, J. Slow Dynamic Processes in Lead Halide Perovskite Solar Cells. Characteristic Times and Hysteresis. *J. Phys. Chem. Lett.* **2014**, *5*, 2357–2363.
- (21) Juarez-Perez, E. J.; Sanchez, R. S.; Badia, L.; Garcia-Belmonte, G.; Kang, Y. S.; Mora-Sero, I.; Bisquert, J. Photoinduced Giant Dielectric Constant in Lead Halide Perovskite Solar Cells. *J. Phys. Chem. Lett.* **2014**, *5*, 2390–2394.
- (22) Almora, O.; Zarazua, I.; Mas-Marza, E.; Mora-Sero, I.; Bisquert, J.; Garcia-Belmonte, G. Capacitive Dark Currents, Hysteresis, and Electrode Polarization in Lead Halide Perovskite Solar Cells. *J. Phys. Chem. Lett.* **2015**, *6*, 1645–1652.
- (23) Hoke, E. T.; Slotcavage, D. J.; Dohner, E. R.; Bowring, A. R.; Karunadasa, H. I.; McGehee, M. D. Reversible Photo-induced Trap Formation in Mixed-halide Hybrid Perovskites for Photovoltaics. *Chem. Sci.* **2015**, *6*, 613–617.
- (24) Snaith, H. J.; Abate, A.; Ball, J. M.; Eperon, G. E.; Leijtens, T.; Noel, N. K.; Stranks, S. D.; Wang, J. T.-W.; Wojciechowski, K.; Zhang, W. Anomalous Hysteresis in Perovskite Solar Cells. *J. Phys. Chem. Lett.* **2014**, *5*, 1511–1515.
- (25) Shao, Y.; Xiao, Z.; Bi, C.; Yuan, Y.; Huang, J. Origin and Elimination of Photocurrent Hysteresis by Fullerene Passivation in $\text{CH}_3\text{NH}_3\text{PbI}_3$ Planar Heterojunction Solar Cells. *Nat. Commun.* **2014**, *5*, 5784.
- (26) Wojciechowski, K.; Stranks, S. D.; Abate, A.; Sadoughi, G.; Sadhanala, A.; Kopidakis, N.; Rumbles, G.; Li, C.-Z.; Friend, R. H.; Jen, A. K. Y.; Snaith, H. J. Heterojunction Modification for Highly Efficient Organic-Inorganic Perovskite Solar Cells. *ACS Nano* **2014**, *8*, 12701–12709.
- (27) Xu, J.; Buin, A.; Ip, A. H.; Li, W.; Voznyy, O.; Comin, R.; Yuan, M.; Jeon, S.; Ning, Z.; McDowell, J. J.; Kanjanaboos, P.; Sun, J.-P.; Lan, X.; Quan, L. N.; Kim, D. H.; Hill, I. G.; Maksymovych, P.; Sargent, E. H. Perovskite-fullerene Hybrid Materials Suppress Hysteresis in Planar Diodes. *Nat. Commun.* **2015**, *6*, 7081.
- (28) Dualeh, A.; Moehl, T.; Tetreault, N.; Teuscher, J.; Gao, P.; Nazeeruddin, M. K.; Grätzel, M. Impedance Spectroscopic Analysis of Lead Iodide Perovskite-Sensitized Solid-State Solar Cells. *ACS Nano* **2014**, *8*, 4053–4053.
- (29) Christians, J. A.; Manser, J. S.; Kamat, P. V. Best Practices in Perovskite Solar Cell Efficiency Measurements. Avoiding the Error of Making Bad Cells Look Good. *J. Phys. Chem. Lett.* **2015**, *6*, 852–857.
- (30) Haruyama, J.; Sodeyama, K.; Han, L. Y.; Tateyama, Y. First-Principles Study of Ion Diffusion in Perovskite Solar Cell Sensitizers. *J. Am. Chem. Soc.* **2015**, *137*, 10048–10051.
- (31) Eames, C.; Frost, J. M.; Barnes, P. R. F.; O'Regan, B. C.; Walsh, A.; Islam, M. S. Ionic Transport in Hybrid Lead Iodide Perovskite Solar Cells. *Nat. Commun.* **2015**, *6*, 7497.
- (32) Azpiroz, J. M.; Mosconi, E.; Bisquert, J.; De Angelis, F. Defect Migration in Methylammonium Lead Iodide and Its Role in Perovskite Solar Cell Operation. *Energy Environ. Sci.* **2015**, *8*, 2118–2127.

(33) O'Regan, B. C.; Barnes, P. R. F.; Li, X.; Law, C.; Palomares, E.; Marin-Belouqui, J. M. Optoelectronic Studies of Methylammonium Lead Iodide Perovskite Solar Cells with Mesoporous TiO₂: Separation of Electronic and Chemical Charge Storage, Understanding Two Recombination Lifetimes, and the Evolution of Band Offsets during J-V Hysteresis. *J. Am. Chem. Soc.* **2015**, *137*, 5087–5099.

(34) Tress, W.; Marinova, N.; Moehl, T.; Zakeeruddin, S. M.; Nazeeruddin, M. K.; Grätzel, M. Understanding the Rate-dependent J-V Hysteresis, Slow Time Component, and Aging in CH₃NH₃PbI₃ Perovskite Solar Cells: the Role of a Compensated Electric Field. *Energy Environ. Sci.* **2015**, *8*, 995–1004.

(35) Zhang, H.; Liang, C.; Zhao, Y.; Sun, M.; Liu, H.; Liang, J.; Li, D.; Zhang, F.; He, Z. Dynamic Interface Charge Governing the Current-voltage Hysteresis in Perovskite Solar Cells. *Phys. Chem. Chem. Phys.* **2015**, *17*, 9613–9618.

(36) Zhao, Y.; Liang, C.; Zhang, H.; Li, D.; Tian, D.; Li, G.; Jing, X.; Zhang, W.; Xiao, W.; Liu, Q.; Zhang, F.; He, Z. Anomalous Large Interface Charge in Polarity-switchable Photovoltaic Devices: an Indication of Mobile Ions in Organic-inorganic Halide Perovskites. *Energy Environ. Sci.* **2015**, *8*, 1256–1260.

(37) Stumpp, M.; Ruess, R.; Horn, J.; Tinz, J.; Richter, C.; Schlettwein, D. I-V Hysteresis of Methylammonium Lead Halide Perovskite Films on Microstructured Electrode Arrays: Dependence on Preparation Route and Voltage Scale. *Phys. Status Solidi A* **2015**, DOI: 10.1002/pssa.201532527.

(38) Kutes, Y.; Ye, L. H.; Zhou, Y. Y.; Pang, S. P.; Huey, B. D.; Padture, N. P. Direct Observation of Ferroelectric Domains in Solution-Processed CH₃NH₃PbI₃ Perovskite Thin Films. *J. Phys. Chem. Lett.* **2014**, *5*, 3335–3339.

(39) Wei, J.; Zhao, Y. C.; Li, H.; Li, G. B.; Pan, J. L.; Xu, D. S.; Zhao, Q.; Yu, D. P. Hysteresis Analysis Based on the Ferroelectric Effect in Hybrid Perovskite Solar Cells. *J. Phys. Chem. Lett.* **2014**, *5*, 3937–3945.

(40) Chen, H.-W.; Sakai, N.; Ikegami, M.; Miyasaka, T. Emergence of Hysteresis and Transient Ferroelectric Response in Organo-Lead Halide Perovskite Solar Cells. *J. Phys. Chem. Lett.* **2015**, *6*, 164–169.

(41) Chen, B.; Zheng, X. J.; Yang, M. J.; Zhou, Y.; Kundu, S.; Shi, J.; Zhu, K.; Priya, S. Interface Band Structure Engineering by Ferroelectric Polarization in Perovskite Solar Cells. *Nano Energy* **2015**, *13*, 582–591.

(42) van Reenen, S.; Kemerink, M.; Snaith, H. J. Modeling Anomalous Hysteresis in Perovskite Solar Cells. *J. Phys. Chem. Lett.* **2015**, *6*, 3808–3814.

(43) Xiao, Z.; Yuan, Y.; Shao, Y.; Wang, Q.; Dong, Q.; Bi, C.; Sharma, P.; Gruverman, A.; Huang, J. Giant Switchable Photovoltaic Effect in Organometal Trihalide Perovskite Devices. *Nat. Mater.* **2015**, *14*, 193–198.

(44) Tao, C.; Neutzner, S.; Colella, L.; Marras, S.; Srimath Kandada, A. R.; Gandini, M.; De Bastiani, M.; Pace, G.; Manna, L.; Caironi, M.; Bertarelli, C.; Petrozza, A. 17.6% Stabilized Efficiency in Low-temperature Processed Planar Perovskite Solar Cells. *Energy Environ. Sci.* **2015**, *8*, 2365–2370.

(45) Xiao, Z. G.; Bi, C.; Shao, Y. C.; Dong, Q. F.; Wang, Q.; Yuan, Y. B.; Wang, C. G.; Gao, Y. L.; Huang, J. S. Efficient, High Yield Perovskite Photovoltaic Devices Grown by Interdiffusion of Solution-processed Precursor Stacking Layers. *Energy Environ. Sci.* **2014**, *7*, 2619–2623.